UC Merced

UC Merced Previously Published Works

Title

Effect of Ion Pair on Contact Angle for Phosphonium Ionic Liquids

Authors

Liu, Ting
Rahman, Hafizur
Menezes, Pradeep L
et al.

Supplemental Material

https://escholarship.org/uc/item/8vn1t2p7#supplemental

Peer reviewed

Effect of Ion Pair on Contact Angle for Phosphonium Ionic Liquids

Ting Liu,[†] Md Ha izur Rahman,[‡] Pradeep L. Menezes,[‡] and Ashlie Martini[*,†]

[†]*Department of Mechanical Engineering, University of California Merced, 5200 Lake Rd, Merced, 95343, CA, USA*

[‡]*Department of Mechanical Engineering, University of Nevada Reno, 1664 N Virginia St, 89557, Reno, NV, USA*

E-mail: amartini@ucmerced.edu

Phone: +1 (209) 228-2354

Abstract

The wettability of ionic liquids (ILs) is relevant to their use in various applications. However, a mechanistic understanding of how the cation-anion pair affects wettability is still evolving. Here, focusing on phosphonium ILs, wettability was characterized in terms of contact angle using experiments and classical molecular dynamics simulations. Both experiments and simulations showed that contact angle was affected by the anion and increased as benzoate < salicylate < saccharinate. Further, the simulations showed contact angle decreased with increased alkyl chain length for these anions paired with five different tetra-alkyl-phosphonium cations. The trends were explained in terms of adhesive and cohesive energies in the simulations, and then correlated to the atomic scale differences between the anions and cations.

Introduction

Ionic liquids (ILs) are salts in the liquid state below 100°C, or even at room temperature (25°C).[1] ILs have a unique combination of physico-chemical properties, including low vapor pressure or non-volatility, long range of solubility, tunable acidity and basicity, high thermal stability, high ion conductivity, and wide electrochemical window, etc.[1,2] These properties enable ILs to be used as organic solvents, mineral acids, bases, catalysts, and many more for a diverse range of applications.[1–6]

ILs comprise a positively charged cation and negatively charged anion. A wide variety of anions, both organic and inorganic, are used in application-relevant ILs, but cations are usually organic species such as ammonium, phosphonium, imidazolium, or pyridinium.[1,7] Among these ILs, phosphonium ILs have been reported to have low wear and friction as lubricants,[8,9] high chemical and thermal stability,[10,11] as well as superior resistance to corrosion.[12–14] Importantly, many halogen-free phosphonium ILs are considered environmentally friendly,[15–17] since they are biodegradable and can be extracted from bio-based feedstock.[5,18–20] Therefore, phosphonium ILs are used as lubricants/lubricant additives,[21–26] battery electrolytes,[27–29] heat transfer fluids,[30,31] solvents for coating materials,[32,33] and additives in polymeric materials.[34–38]

In many applications, phosphonium ILs are in contact with a solid surface and form a solid-liquid interface. Therefore, the adsorption and spreading of phosphonium ILs on solid surfaces, i.e., wettability, plays an important role in their performance.[39–41] Wettability is controlled by the balance between the intermolecular adhesion (liquid-solid) and cohesion (liquid-liquid) interactions.[42] For phosphonium ILs used as lubricants, wettability is important because it affects the fluid's ability to spread and protect solid surfaces.[40,43] Wetting is also important for phosphonium ILs used as electrolytes since the utilization rate of electrode surface area and energy density of supercapacitors can be improved by increasing wettability.[44]

Usually, wettability is quantified as the contact angle between a liquid droplet and a

solid surface.[45] Strong adhesion to the substrate surface and weak cohesion within the liquid lead to a high degree of wetting with low contact angles, while a combination of weak adhesion and strong cohesion results in high contact angles and poor wetting. When a droplet is placed on a surface, there is initially transient evolution of contact angle as the liquid droplet is wetting the surface and then the contact angle reaches steady state. Both the transient and steady-state contact angles are used to characterize wetting behavior. Usually, a steady-state contact angle less than 90° indicates good wettability.[46] Wetting time, the time required for the contact angle to reach steady state, can be used to determine the relative strengths of adhesion and cohesion. Longer wetting times indicate adhesion domination, whereas shorter wetting times indicate the dominance of cohesion.[47] These properties can be measured experimentally using a goniometer as well as with molecular dynamics (MD) simulations that give an atomistic view of contact angle mechanisms.

Experimental studies have reported the contact angle of neat phosphonium ILs measured on a variety of surfaces and at a range of temperatures. All reported good wettability with contact angles less than 90°.[39,40,47–51] Some studies have compared contact angles on different substrates and shown that wettability is better on materials with high surface free energy, i.e, lower contact angle on steel than PTFE[49] and lower contact angle on TiN than steel, CrN, and ZrN.[40] Temperature has also been shown to affect contact angle. However, while the contact angle of some ILs decreases with increasing temperature,[39] other ILs exhibit the opposite trend.[47] Lastly, the wettability of phosphonium ILs in solution has also been measured experimentally and it has been reported that contact angles of IL solutions could be smaller or larger than those of the neat ILs, depending on the solvent and substrate material.[22,52]

MD simulations have been used to complement experiments by exploring the atomistic origins of IL wettability.[53–58] However, currently there are few simulation studies focused on the wettability of phosphonium ILs. Simulations showed that the steady state contact angle of [P4,4,4,4][Cpy] on silanol and silane surfaces was less than 90°, indicating a strong

3

liquid-surface interaction, but the contact angle was slightly larger on the silane surface.[59] The steady-state contact angle of [P2,2,2,5][Tf$_2$N] nanodroplets on platinum surfaces at 298 K was calculated in simulations. The results showed that the contact angle on Pt(100) was higher than on Pt(111), demonstrating that the crystallographic nature of the surface can affect spreading. The simulations also compared two different ILs and found that the contact angle of [P2,2,2,5][Tf$_2$N] nanodroplets was lower than that of its ammonium counterpart [N2,2,2,5][Tf$_2$N] on both Pt surfaces.[58]

IL properties, including wettability, are significantly affected by the chemistry and structure of the cation and anion combination.[5,60] No previous studies of phosphonium ILs focused on the effect of the cation. However, some studies that characterized the effect of cation for other ILs reported that longer alkyl chains correspond to lower contact angle. For example, the contact angle of [TF$_2$N] anion-based ILs with different cations was experimentally found to be lower for longer alkyl chain with contact angle increasing as [C$_{10}$C$_1$im] < [C$_4$C$_1$im] < [C$_2$C$_1$im].[54] This trend was consistent with simulation results that showed radial distribution function (RDF) peaks were sharper and higher for longer chains, indicating better ordering near the surface.[54] In another simulation study, the contact angle of [BF$_4$]-based ILs on graphite surface was lower for [PrMIM] cation with a longer alkyl chain compared to [DMIM] cation with a shorter alkyl chain. The interaction energy between graphite and [PrMIM][BF$_4$] was found to be higher than that for [DMIM][BF$_4$] which implied that the longer [PrMIM] cations had a stronger affinity towards the graphite surface, leading to a lower contact angle.[55] Lastly, simulations showed that contact angles of ILs with [BMIM] with long alkyl chains were lower than [EMIM] ILs with short chains for anions including [Cl], [Br], [BF$_4$], [PF$_6$], and [TF$_2$N] on bismuth telluride surfaces .[57]

For the effect of anion, it was reported that, for [P6,6,6,14] cations, contact angle increased as [p-TsO] < [Tf$_2$N] < [Cl] < [DCA] < [BF$_4$] on PTFE surfaces. The lower contact angle of [p-TsO] was attributed to the planarity and electron density of the aromatic ring.[50] An experimental study reported that contact angle increased as [BEHP] < [(iC8)$_2$PO$_2$] < [Cl] <

[DCA] on AISI 52100 steel, CrN, and ZrN surface for the same [P6,6,6,14] cation. This trend was attributed to the inverse relationship between anion size and surface tension.[40] The effect of anion size was also observed in simulations of non-phosphonium ILs that showed larger anions had better wetting on bismuth telluride surfaces and the contact angle decreased as [Cl] > [Br] > [BF$_4$] > [PF$_6$] > [TF$_2$N] for imidazolium-based ([BMIM] and [EMIM]) ionic liquids. This trend was attributed to higher cohesion energy for the larger anions.[57]

Results reported so far have shown that cation and anion can affect wettabilty, but there has been no systematic study of these effects for phosphonium ILs nor the underlying mechanisms. Here we explored the relationship between phosphonium cation-anion pairs and contact angle. In particular, the effect of different anions (especially with similar chemistries) for the same cation and the effect of alkyl chain length in tetra-alkyl-phosphonium cations for the same anion were studied. Although wetting behavior depends on the surface material and morphology as well,[58] here we focus on the effects of the cation and anion. First, the wettability of three ionic liquids with benzoate [Benz], salicylate [Sali], and saccharinate [Sacc] anions paired with [P6,6,6,14] cation was experimentally measured on 52100 stainless steel. The contact angle for these phosphonium ILs on a model iron surface was calculated by MD simulations to confirm the trend observed in experiments. The simulations were extended to characterize the effect of the cation using ILs with [P4,4,4,4], [P4,4,4,8], [P4,4,4,14], [P6,6,6,14], and [P8,8,8,14] cations. Finally, the origins of observed cation and anion trends were explored in terms of the strength of the adhesion and cohesion interactions.

Methods

Experiments

Three ILs were synthesized through ion exchange reactions using [P6,6,6,14] chloride, and either sodium saccharinate, sodium salicylate, or sodium benzoate, following the process described previously by Reeves et al.[61] and other researchers,[62,63] to yield, [P6,6,6,14][Sacc],

5

[P6,6,6,14][Sali], and [P6,6,6,14][Benz]. Mirror finished AISI 52100 stainless steel surface was prepared using silicon carbide polishing papers of 120, 240, 400, 600, 1000 grit size followed by diamond suspension of 6 μm, 3 μm, and 1 μm. The average surface roughness (Ra=17.9±4.9 nm) was measured using an optical profilometer (Rtec, CA, USA), with 10x magnification using white light interferometry.

The contact angle measurements of the three phosphonium ILs were carried out using a goniometer (Rame-hart Model-260, NJ, USA). A 5 μL sessile droplet of each liquid was deposited on the surface using a microsyringe assembly with a SS 304, straight, 22 gauge needle with (part number 100-10-12-22), and the droplet was imaged using a camera with 750 FPS superspeed U2 series upgrade kit (part number 100-12-U2), all manufactured by Rame-hart. Contact angle was calculated as the angle between the line along stainless steel surface and the tangential line to the droplet surface. The contact angles on either side of the sessile droplet were recorded every 1 second interval, using Dropimage software, and the average of the contact angle on the two sides of the droplet (θ) was tracked over time. Each test was repeated three times.

Molecular Dynamics Simulation

Since the alkyl chain length in cations affect contact angle, the simulations were extended beyond the IL systems studied experimentally to include five different cations [P4,4,4,4], [P4,4,4,8], [P4,4,4,14], [P6,6,6,14], and [P8,8,8,14] in combination with three anions [Benz], [Sali], and [Sacc]. Snapshots of the individual ions are shown in Fig 1. Each simulation had one IL droplet on a 250 × 250 Å square surface comprising five layers of Fe atoms arranged in a body-centered-cubic lattice with (111) orientation with the bottom layer fixed, as shown in Fig. 2.

The interatomic interactions within and between the ILs were described by the OPLS-AA Force field[64] based on LigParGen.[65] Interactions with the iron substrate were modeled using the Lennard-Jones (LJ) potential with $\epsilon_{ss} = 0.2007$ eV and $\sigma_{ss} = 2.4193$ Å.[66] Interactions

6

[P8,8,8,14]

[P6,6,6,14]

[P4,4,4,14]

[P4,4,4,8]
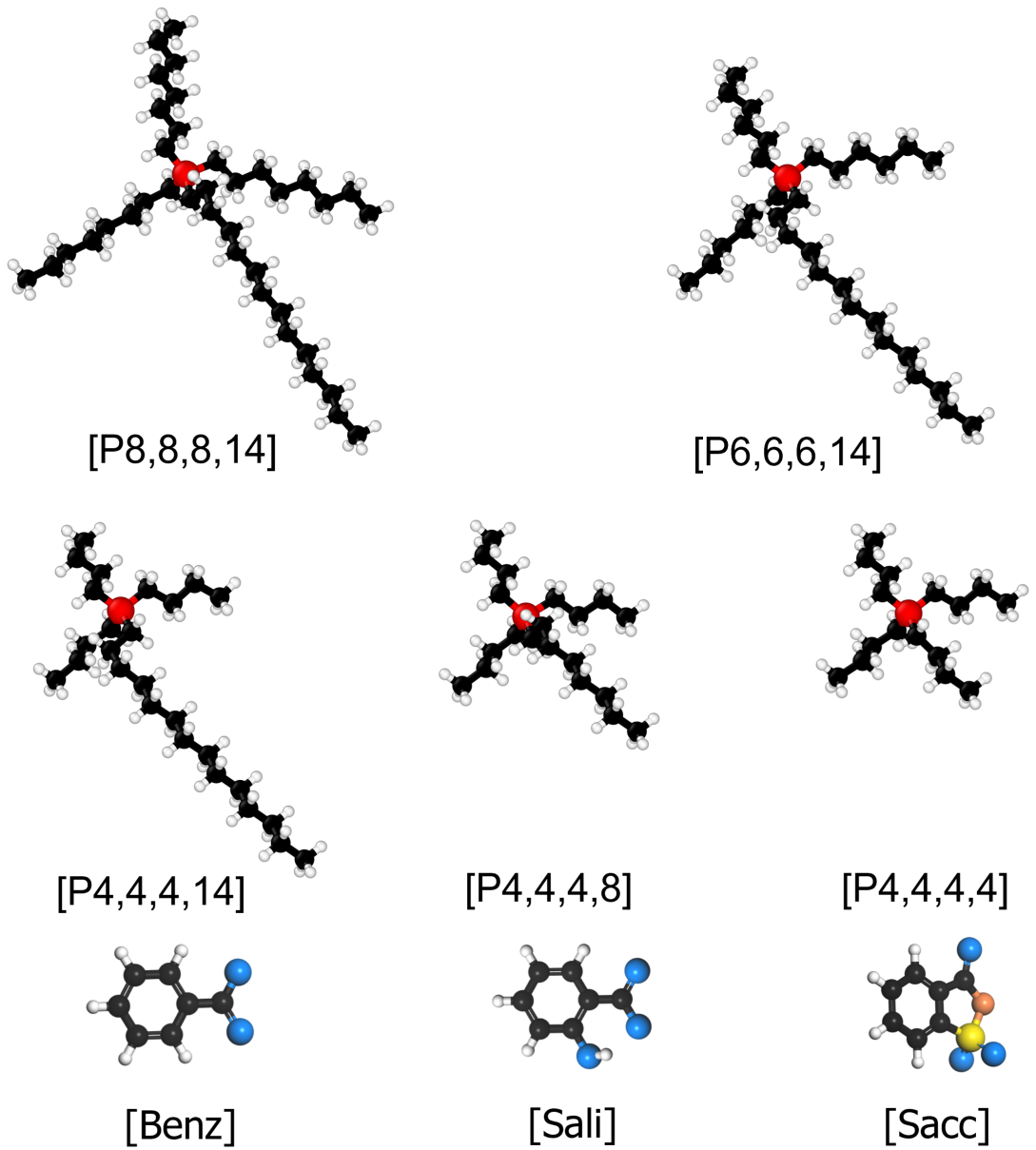
[P4,4,4,4]

[Benz]

[Sali]

[Sacc]

Figure 1: Snapshots of the molecular models of the five cations and three anions used in the simulations of phosphonium ILs. Sphere colors correspond to atoms type: white H, black C, red P, blue O, orange N, and yellow S.

[145] between substrate and ILs were modeled using the LJ potential, combining the Fe parameters

[146] with the LJ parameters of OPLS-AA using geometric mixing rules.[67]

[147] It has been found that contact angle generally increases linearly with droplet size until it

[148] converges to a constant values after a critical number of ions or droplet radius is reached.[68,69]

[149] In previous simulations, the contact angle was found to converge for [BMIM][BF$_4$] on graphene

[150] with at least 100 ion pairs[69] or an initial cubic box size of 50 Å[55] and for [EMIM][BF$_4$] on

[151] silicon with a droplet radius of at least 20 Å.[70] Based on these, all model phosphonium IL

[152] systems here were created using PACKMOL[71] with at least 100 ion pairs, corresponding

[153] to the liquid in a 50 Å cubic volume. The IL cube was initially placed 10 Å above iron

[154] surface. All MD simulations were performed using the open-source Large Atomic/Molecular

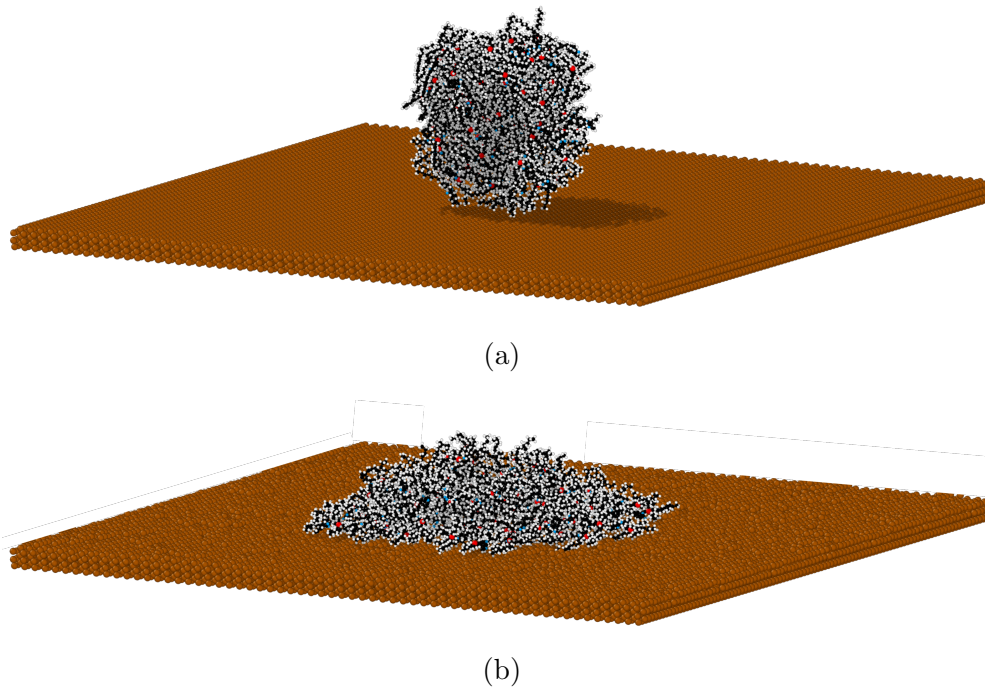[155] Massively Parallel Simulation (LAMMPS) package[72] with a timestep of 1 fs.

(a)

(b)

Figure 2: Perspective view snapshots of (a) the model IL droplet contacting the surface and (b) after 10 ns of relaxation for [P6,6,6,14][Benz].

[156] First, energy minimization was performed using the conjugate gradient algorithm until

[157] reaching a stopping tolerance of 1.0×10^{-6} for energy and 1.0×10^{-8} for force. After energy

8

minimization, the IL was partially relaxed as the temperature was increased from 1 K to 298 K over 1 ns in a canonical ensemble (NVT). The Nosé–Hoover thermostat[73] was used to control the temperature of the system and the velocity-Verlet algorithm[74] was applied to solve the equations of motion. This relaxation procedure ensured the cohesion in the ionic liquid and droplet formation. During this relaxation stage, the cube IL droplet became a more physically realistic spherical shape and came into contact with the substrate surface, as shown in Fig. 2(a). Then, the production simulation was run at temperature of 298 K for another 10 ns. The droplet spread on the surface starting from the initial point of contact between the droplet and surface, finally reaching a steady state shape like that shown in Fig. 2(b). Each simulation was run three times from the same atomic configuration with different initial velocity distributions.

In previous simulation studies,[57–59] the contact angle was determined using a simple two-dimension method as the angle between the horizontal line at the liquid-solid interface and the line tangent to the droplet surface at the liquid-solid-valor three phase contact point. This calculation has also been performed using more complicated three-dimensional algorithms.[70,75,76] However, the tangent line is difficult to define for the relatively large and branched ions here. Therefore, the contact angle was determined by the equation $\theta = tan^{-1}(h/r)$, where r is the radius of the liquid-solid contact circle and the h is the height of the apex;[53,77] details of the contact angle calculation are given in Fig. S1. After the potential energy reached steady state, the contact angle was calculated by averaging 20 trajectories (time steps) during the last 1 ns of the simulation.

Throughout the simulation, the adhesive and cohesive energies were calculated from the sum of the energies between individual atom pairs. Adhesion energy was calculated as the sum of the energy between atoms in the anion or cation and the Fe atoms in the substrate; cohesion energy was calculated as the total interaction energy between atoms in the anion and cation. These summed energies were averaged over the last 1 ns of the production simulations, consistent with the contact angle calculation. A negative adhesive or cohesive

9

energy corresponds to net attraction.

Results and Discussion

Comparison of Experiments and Simulations

The ILs measured experimentally comprised [P6,6,6,14] with three different anions. As shown in Fig. 3(a), the contact angle of all three ILs decreased rapidly to approach a steady-state value. At steady state, the contact angles of [P6,6,6,14][Sacc], [P6,6,6,14][Sali], and [P6,6,6,14][Benz] were 14.2°, 6.89°, and 4.10°, respectively. The small contact angles measured here are consistent with previous studies of [P6,6,6,14][Tf$_2$N] ILs on stainless steel surface ,[47,51] which also reported contact angles less than 20°. Generally, the results indicate that all three phosphonium ILs have a good wettability on stainless steel.
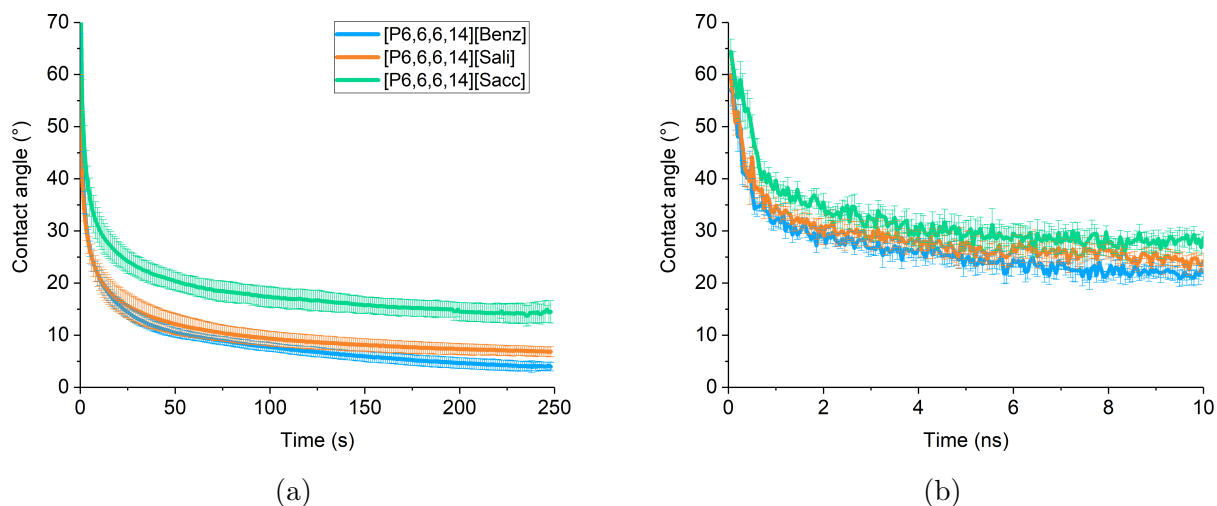

Figure 3: Contact angle as a function of time for [P6,6,6,14][Benz], [P6,6,6,14][Sacc], and [P6,6,6,14][Sali] from (a) experimental measurements on polished AISI 52100 steel surface with error bars reflecting the standard deviation across four independent measurements; and (b) simulation calculations on Fe (111) surface with error bars reflecting the standard deviation across three independent MD simulations.

Among the three ILs, [P6,6,6,14][Sacc] had the largest contact angle, more than twice that of [P6,6,6,14][Sali] and [P6,6,6,14][Benz], over the entire spreading time. For [P6,6,6,14][Sali]

and [P6,6,6,14][Benz], the contact angles were not statistically different during the transient phase but, at steady state, [P6,6,6,14][Sali] had a larger contact angle. These results indicate that the anion can affect contact angle, as observed in previous studies.[39,47–49,51,78]

MD simulations were carried out for the same three [P6,6,6,14]-based ILs characterized experimentally. As shown in Fig. 3(b), the contact angle of all the three ILs gradually decreased during the 10 ns simulation. The average contact angles over the last 1 ns of the simulation for [P6,6,6,14][Sacc], [P6,6,6,14][Sali], and [P6,6,6,14][Benz] were 28.1°, 24.3°, and 21.8°, respectively. The magnitudes of the simulation contact angles were larger than those in experiment due to the limited size and time scales of the simulations. Also, note that the time scale of the experiments in Fig. 3(a) is seconds while that of the simulations in Fig. 3(b) is nanoseconds, so the results cannot be directly compared. However, despite their differences, in both simulations and experiments, [P6,6,6,14][Sacc] had the largest steady-state contact angle and [P6,6,6,14][Benz] had the smallest.

As mentioned in the Introduction, both the cation and anion can affect wettability. The simulations were used to explore this further by comparing the contact angle for ILs with the three anions characterized above combined with five different cations. The effects of the cations and anions were analyzed separately, with trends investigated in terms of adhesive and cohesive energies.

Effect of Cations

The steady-state contact angle is plotted with respect to cation in Fig 4. It is observed that steady-state contact angles decreased with increasing alkyl chain length for all three anions. This trend was also reported in previous studies for imidazolium cations.[54,55,57] Another observation in Fig 4 is that contact angle decreased with increasing cation size, regardless of whether the size increase was in one chain (compare [P4,4,4,4], [P4,4,4,8], and [P4,4,4,14]) or multiple chains ([P4,4,4,14], [P6,6,6,14], and [P8,8,8,14]). The overall trend may be due to the longer chains increasing adhesion or decreasing cohesion, or both.
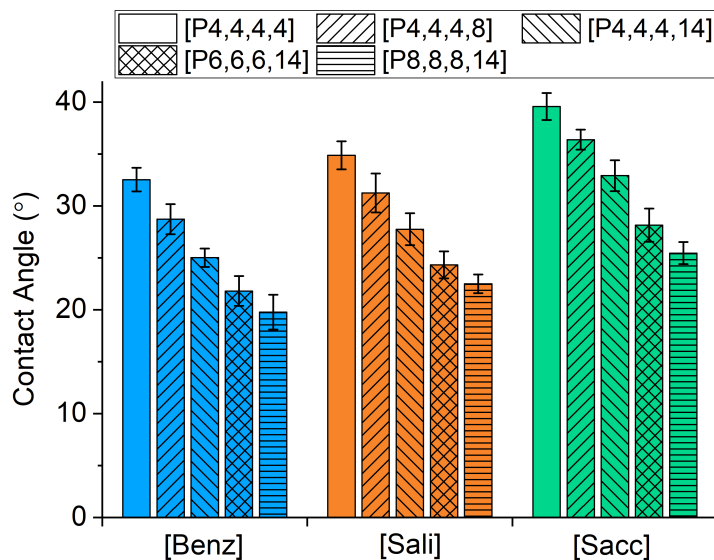
11

Figure 4: Comparison of the steady state contact angle for cations with different alkyl chain lengths paired with three different anions. Error bars reflect standard deviation among three independent MD simulations. Data is grouped by anion to highlight the effect of the cation.
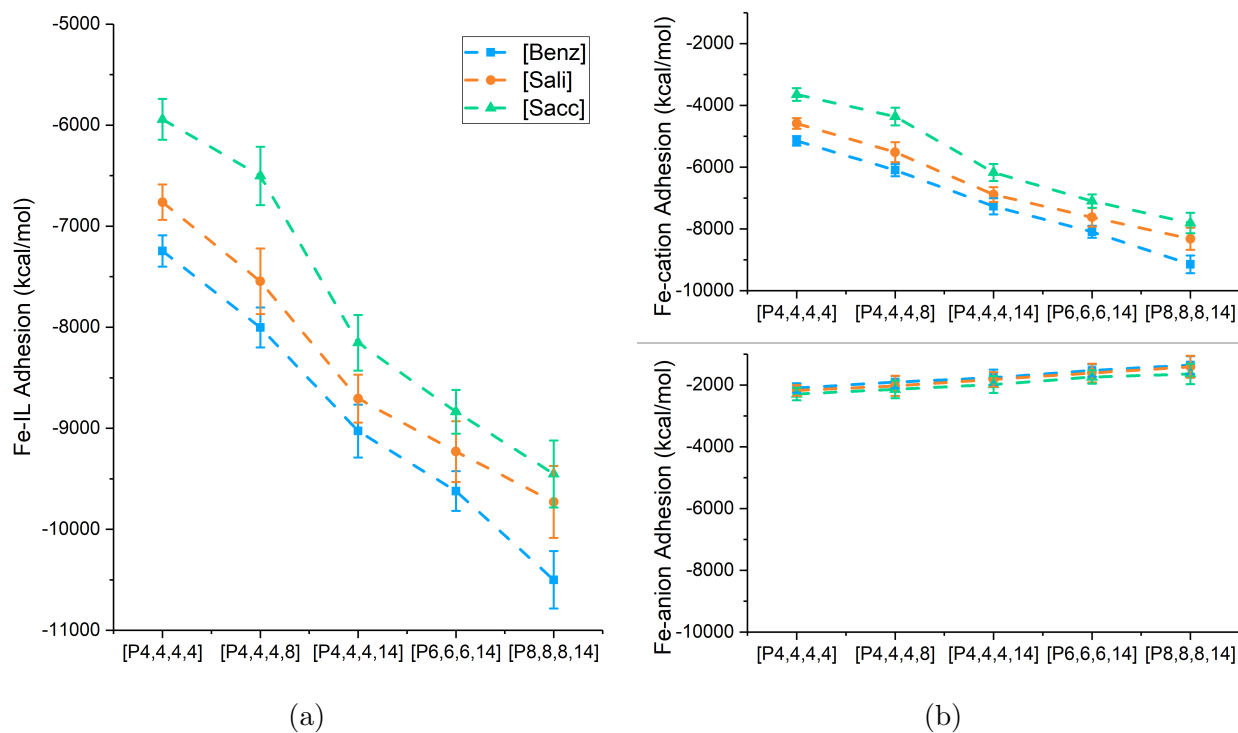

(a)

(b)

Figure 5: Adhesive interaction energy between the surface and the ILs, and (b) separated into the cation (top) and anion (bottom) contributions, plotted as functions of increasing alkyl chain length for the three anions.
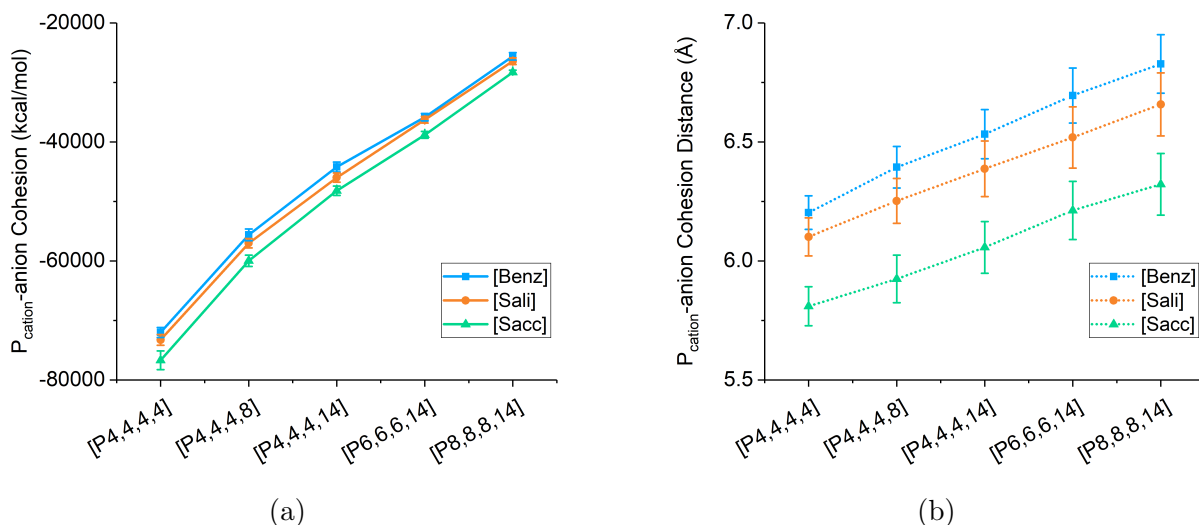
Figure 6: (a) Cohesive energy between P atoms in the cations and all atoms in the anions, and (b) average distance between cation P atoms and the COM of the anions, plotted as functions of increasing alkyl chain length for the three anions.

The total Fe-IL adhesion energy, reported in Fig. 5(a), increased (became more negative) with increasing cation chain length, consistent with the trend of decreasing contact angle. The adhesive energy was separated into contributions from the cation and anion, as shown in Fig. 5(b). The Fe-cation adhesive energy increased with chain length while the Fe-anion energy decreased with chain length. However, the magnitude of the cation adhesion was much larger than that for the anion, so the cation trend dominated the overall adhesion with the surface. The Fe-cation interaction energy was further broken down by atom type (Fig. S2) and it was found that the C atoms contribute most to the total adhesion. Therefore, the increasing adhesive energy trend can be attributed to the fact that there are more C atoms present in the longer chains.

The cohesion between ions was also analyzed. It was found that the only attractive inter-ionic interactions were between the P atoms in the cation and the atoms in the anions (Fig. S3). The cohesive energy between the cation P atoms and the anions, shown in Fig. 6(a), decreased (becomes less negative) with increasing chain length. The trend could be due to the interference of the longer chains that separated the anion and cation, thereby decreasing

cohesion. This hypothesis was confirmed by calculating the average distance between the cation P atom and the center-of-mass (COM) of the nearest anion. As shown in Fig. 6(b), the cation-anion distance increased with alkyl chain length, consistent with the decreasing cohesive energy and the corresponding lower contact angle.

Effect of Anions

The steady-state contact angles are plotted with respect to anion in Fig. 7. For all five cations, the contact angle increased as [Benz] < [Sali] < [Sacc]. It has been proposed that larger anions will have lower contact angle.[40] Anions with aromatic rings like [p-TsO] have also been reported to have lower contact angle than anions without aromatic rings like [BF$_4$], [DCA], [Cl] and [Tf$_2$N] because of the planarity and delocalised electron density of the ring.[50] However, [Benz], [Sali], and [Sacc] are all aromatic ring-based anions with similar size, so the difference in their contact angles should be attributed to other mechanisms. First, the adhesion and cohesion were analyzed, following the approach used to explain the cation trends.

The total Fe-IL adhesion energy, plotted vs. anion in Fig. 8(a), was largest for [Benz] and smallest for [Sacc]. This trend is consistent with the observation that [Benz] has the lowest contact angle while [Sacc] has the largest contact angle. To explain how the anions affect total adhesion, the Fe-anion and Fe-cation adhesive energy were analyzed separately.

As shown in Fig. 8(b), Fe-anion adhesive energy increases as [Benz] < [Sali] < [Sacc]. This may be due to the fact that [Sacc] has the most atoms and, as shown in Fig. S4, the biggest contribution to adhesion in [Sacc], the S atom, is not present in the other two anions. Similarly, for [Sali], there is one more O atom in the hydroxyl group than [Benz] which could contribute to the higher interaction energy observed for [Sali]. However, this difference in Fe-anion energy is very small compared to the difference between the anions in terms of Fe-cation adhesion. The Fe-cation adhesion is largest for [Benz] and smallest for [Sacc], consistent with the contact angles. Therefore, the anion contact angle trend can
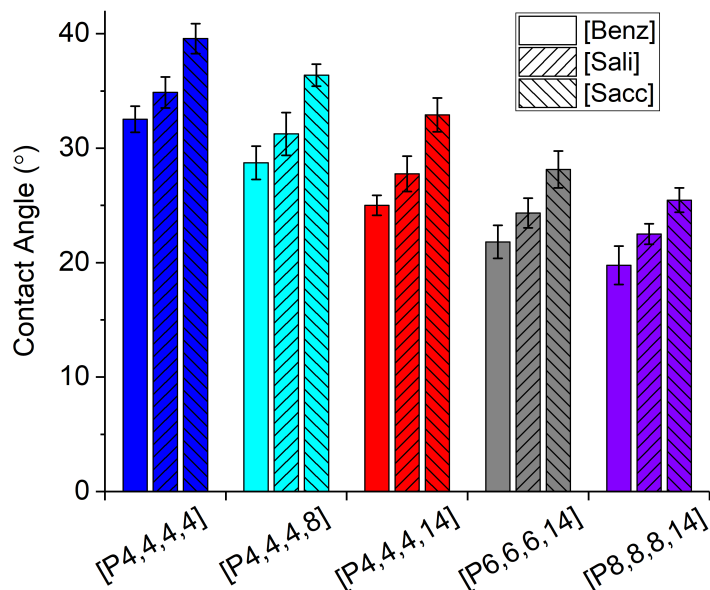
14

Figure 7: Comparison of the steady state contact angle for anions [Benz], [Sali], and [Sacc] paired with five different cations. Error bars reflect standard deviation among three independent MD simulations. Note that this is the same data as in Fig. 4 but shown here with the data grouped by cation to highlight the effect of anion.

be attributed to the indirect effect of the anion on interactions between the cations and substrate.

Since the Fe-anion energy is not very different for the three anions, their effect on cation adhesion may be due to the orientation of the anions with respect to the surface.[79,80] An orientation order parameter[53,55,56] was calculated from the relative directions of the Fe surface-normal and the direction normal to the plane of the anion atoms, as illustrated in Fig. S5. The value of orientation order parameter can vary from -0.5 when the anion ring is parallel to the surface to 1 when the anion ring is perpendicular to the surface. The distributions of the orientation order parameter for anions within 5 Å of the substrate (cutoff distance identified from the first peak of the anion position distribution functions, shown in Fig. S6, were calculated from the last 1 ns of all three independent simulations for each anion. The results for the [P6,6,6,14] cation are shown in Fig. 9, although similar distributions were found for other cations, as shown in Fig. S7 for [P4,4,4,4]. It can be seen that more of the [Benz] anions have an orientation order parameter near 1, meaning they are perpendicular to
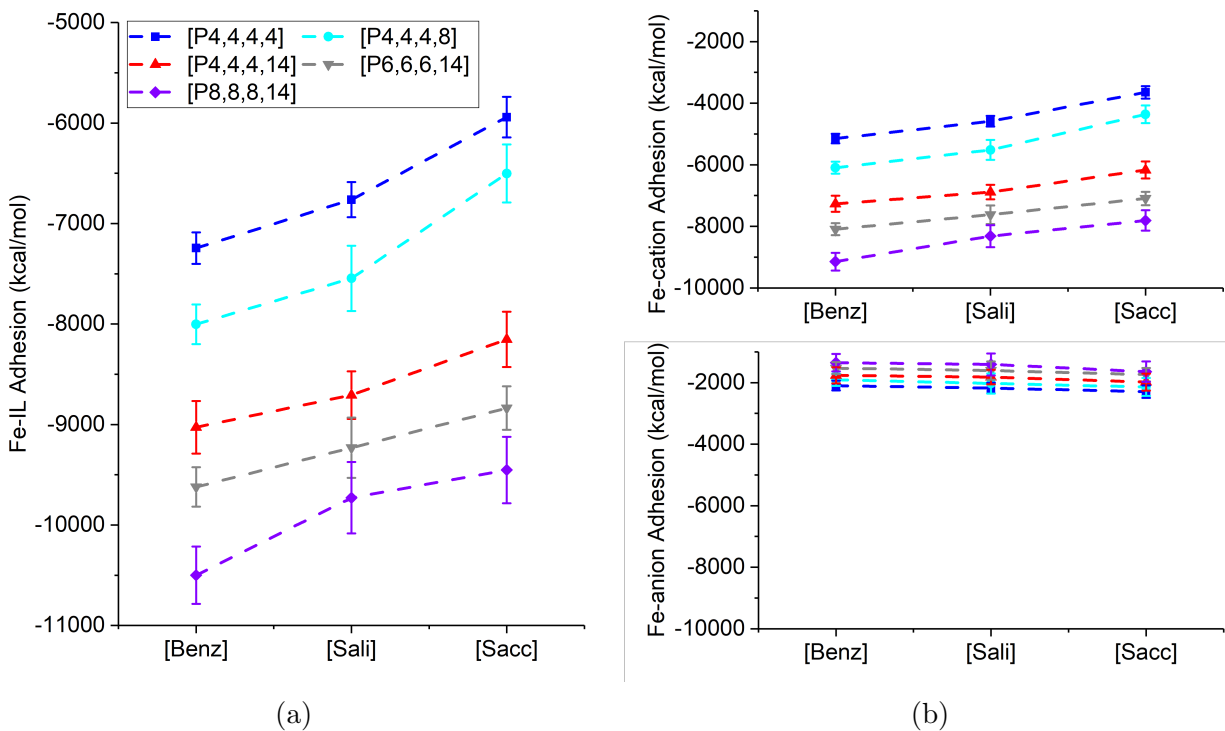
15

(a)

(b)

Figure 8: Adhesive interaction energy between the surface and the ILs, and (b) separated into the cation (top) and anion (bottom) contributions, plotted vs. anion for the five cations. Note that this is the same data as in Fig. 5 but plotted vs. anion to illustrate anion trends.

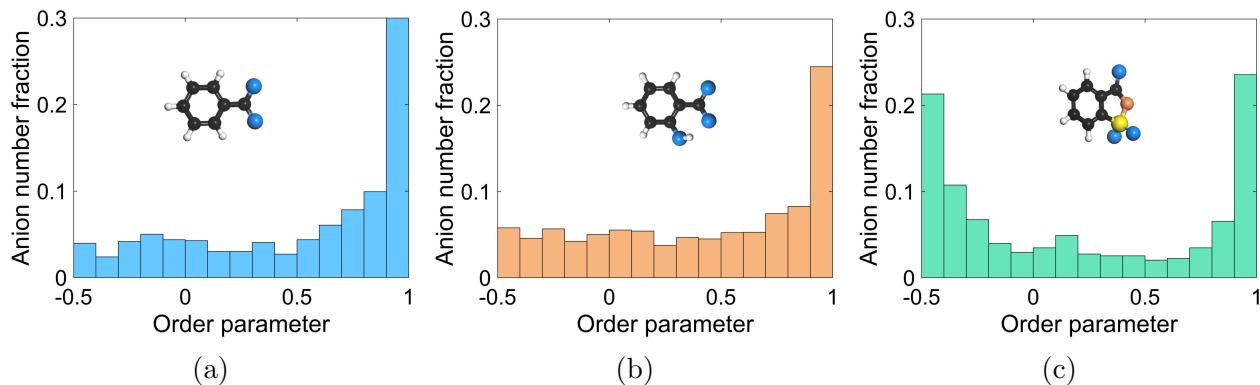(a)   (b)   (c)

Figure 9: Orientation order parameter distribution for (a) [Benz], (b) [Sali], (c) [Sacc] paired with [P6,6,6,14] calculated from the last 1 ns of three independent simulations for each anion. The parameter ranges from -0.5 when the anion ring is parallel to the surface to 1 when the anion ring is perpendicular to the surface.

the surface, whereas the orientation order parameter for the [Sacc] anions is lower, indicating fewer are perpendicular. It has been reported that all three anions can orient perpendicular to metal surfaces,[81–85] but the asymmetry of the [Sacc] anion causes it to tilt towards

16

²⁸¹ the surface.[85] The preferred perpendicular alignment of the [Benz] anions allows the cations

²⁸² more access to the surface, consistent with the stronger Fe-cation adhesion for the [Benz]

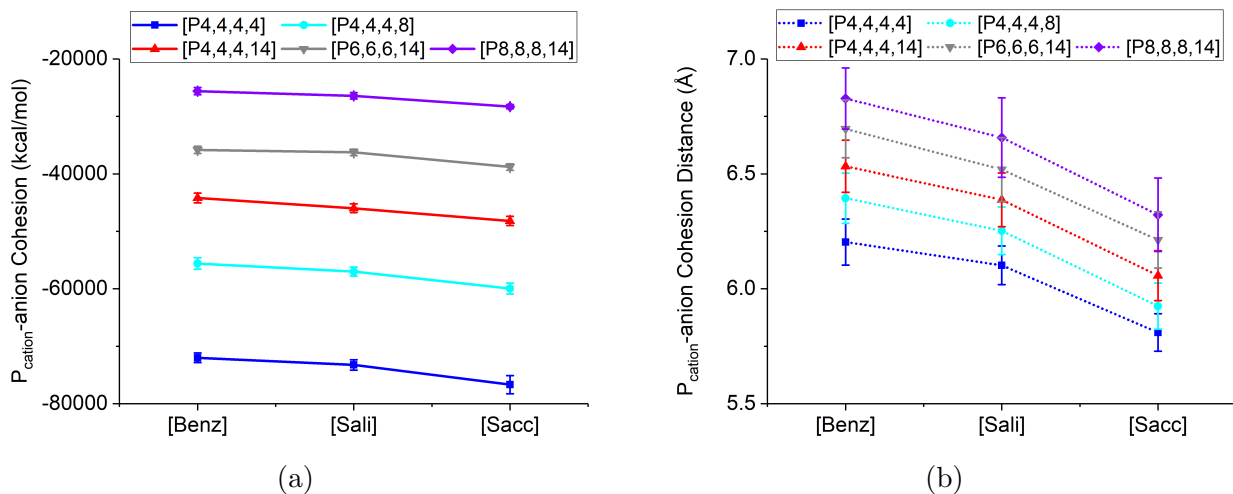²⁸³ ILs than the [Sacc] ILs in Fig. 8(b).

Figure 10: (a) Cohesive energy between P atoms in the cations and all atoms in the anions, and (b) average distance between cation P atoms and the COM of the anions, plotted vs. anions for the five cations. Note that this is the same data as in Fig. 6 but plotted vs. anion to illustrate anion trends.

²⁸⁴ The cohesive energy between the cation P atoms and anions is plotted vs. anion in

²⁸⁵ Fig. 10a. The results show that the cohesion was strongest for [Sacc] and weakest for [Benz]

²⁸⁶ with any cation. This trend was explained by the average distance between the cation P atom

²⁸⁷ and the COM of the nearest anion, in Fig. 10b, that increased as [Sacc] < [Sali] < [Benz]. As

²⁸⁸ presented in Fig. S8, there are more atoms in [Sacc] that have attractive interactions with

²⁸⁹ the cation than the other two anions, and the extra O atom in [Sali] enables stronger cohesion

²⁹⁰ than [Benz]. The cohesion energy and distance trends are consistent with the contact angle

²⁹¹ results.

Conclusions

²⁹³ The wetting of phosphonium ILs with systematically varied cation and anion combinations

²⁹⁴ on ferrous surfaces was evaluated using experiments and MD simulations. Contact angles

of less than 20° in experiments indicated that the ILs have a good wettability on stainless steel, but contact angles are different for [Benz], [Sali], and [Sacc]. The same trend was reproduced in MD simulations. Next, the simulations were extended to include five different cations [P4,4,4,4], [P4,4,4,8], [P4,4,4,14], [P6,6,6,14], and [P8,8,8,14] in combination with three anions. It was found that longer alkyl chains in the cations led to lower contact angle. This was explained by the effect of more C atoms that both increased adhesion with the substrate and separated the P atom in the cation from the anion, thereby decreasing cohesion. For anions, the contact angle increased as [Benz] < [Sali] < [Sacc] when paired with the same cation. Like the cations, the anion contact angle trend was consistent with cohesion energy, and explained by the number and type of atoms in the anions that had attractive interactions with P atom in the cations. The adhesion energy was also consistent with the anion contact angle trend, but this case was explained by the orientation of the anions with respect to the surface. Specifically, perpendicular anion alignment allowed the cations more access to the surface, thereby increasing adhesion. The alignment trends were associated with asymmetry of the anion structures, where greater symmetry led to more perpendicular alignment, higher cation-Fe adhesion, and lower contact angle.

Overall, the results reported here demonstrate that both the cation and anion affect contact angle through their direct and indirect influence on adhesion and cohesion. Although this study focused on the ions, the simulation-based methods developed may be extended in future work to explore the effects of surface parameters and operating conditions. Also, simulation results for more combinations of cations and anions might be used to develop analytical relationships between IL properties and contact angle. Together with matched experiments, such simulations can provide fundamental understanding of the mechanisms underlying the wettability of ILs.

Ionic Liquid Abbreviations

The following are abbreviations used for cations and anions within the body of the document.

BMIM	1-butyl-3-methylimidazolium
DMIM	1,3-dimethylimidazolium tetra-fluoroborate
EMIM	1-ethyl-3-methylimidazolium
PrMIM	1-propyl-3-methylimidazolium
P4,4,4,4	tetrabutylphosphonium
P4,4,4,8	tributyloctylphosphonium
P4,4,4,14	tributyltetradecylphosphonium
P6,6,6,14	trihexyltetradecylphosphonium
P8,8,8,14	trioctyltetradecylphosphonium
$(iC8)_2PO_2$	bis(2,4,4-trimethylpentyl) phosphinate
BEHP	bis(2-ethylhexyl)phosphate
Benz	benzoate
BF_4	tetrafluoroborate
Br	bromide
Cl	chloride
Cpy	2-cyanopyrrolide
DCA	dicyanamide
DEP	diethylphosphate
PF_6	hexafluorophosphate
PTFE	poly(tetrafluoroethylene)
p-TsO	p-toluene-sulfonate
Sacc	saccharinate
Sali	salicylate
Tf_2N	bis(trifluoromethylsulfonyl)amide

19

Acknowledgement

Supporting Information Available

The following file is available free of charge:

Supporting Information provides additional analysis from MD simulations. Contents include a schematic and detailed explaination of the contact angle calculation, Fe-cation adhesion interaction energy by atom type, C_{cation}-anion and P_{cation}-anion cohesion interaction energy, Fe-anion adhesion interaction energy by atom type, illustration and description of the orientation order parameter calculation, Fe-anion vertical distance distribution, anion orientation order parameter distribution, and P_{cation}-anion cohesion interaction energy by atom type.

References

(1) Singh, S. K.; Savoy, A. W. Ionic liquids synthesis and applications: An overview. *J. Mol. Liq.* **2020**, *297*, 112038.

(2) Joshi, M. D.; Anderson, J. L. Recent advances of ionic liquids in separation science and mass spectrometry. *RSC Adv.* **2012**, *2*, 5470–5484.

(3) Reeves, C. J.; Siddaiah, A.; Menezes, P. L. Ionic liquids: a plausible future of bio-lubricants. *J. Bio- Tribo-Corros.* **2017**, *3*, 18.

(4) Welton, T. Ionic liquids: a brief history. *Biophys. Rev.* **2018**, *10*, 691–706.

(5) Rahman, M. H.; Khajeh, A.; Panwar, P.; Patel, M.; Martini, A.; Menezes, P. L. Recent progress on phosphonium-based room temperature ionic liquids: Synthesis, properties, tribological performances and applications. *Tribol. Int.* **2022**, *167*, 107331.

(6) Koutsoukos, S.; Philippi, F.; Malaret, F.; Welton, T. A review on machine learning algorithms for the ionic liquid chemical space. *Chem. Sci.* **2021**, *12*, 6820–6843.

(7) Moniruzzaman, M.; Kamiya, N.; Goto, M. Activation and stabilization of enzymes in ionic liquids. *Org. Biomol. Chem.* **2010**, *8*, 2887–2899.

(8) Scarbath-Evers, L. K.; Hunt, P. A.; Kirchner, B.; MacFarlane, D. R.; Zahn, S. Molecular features contributing to the lower viscosity of phosphonium ionic liquids compared to their ammonium analogues. *Phys. Chem. Chem. Phys.* **2015**, *17*, 20205–20216.

(9) Naik, P. K.; Paul, S.; Banerjee, T. Physiochemical properties and molecular dynamics simulations of phosphonium and ammonium based deep eutectic solvents. *J. Solution Chem.* **2019**, *48*, 1046–1065.

(10) Maton, C.; De Vos, N.; Stevens, C. V. Ionic liquid thermal stabilities: decomposition mechanisms and analysis tools. *Chem. Soc. Rev.* **2013**, *42*, 5963–5977.

(11) Khajeh, A.; Rahman, M. H.; Liu, T.; Panwar, P.; Patel, M.; Menezes, P. L.; Martini, A. Thermal decomposition of phosphonium salicylate and phosphonium benzoate ionic liquids. *J. Mol. Liq.* **2022**, *352*, 118700.

(12) Yu, B.; Bansal, D. G.; Qu, J.; Sun, X.; Luo, H.; Dai, S.; Blau, P. J.; Bunting, B. G.; Mordukhovich, G.; Smolenski, D. J. Oil-miscible and non-corrosive phosphonium-based ionic liquids as candidate lubricant additives. *Wear* **2012**, *289*, 58–64.

(13) Cai, M.; Yu, Q.; Liu, W.; Zhou, F. Ionic liquid lubricants: When chemistry meets tribology. *Chem. Soc. Rev.* **2020**, *49*, 7753–7818.

(14) Henriques, R. R.; Soares, B. G. Sepiolite modified with phosphonium ionic liquids as anticorrosive pigment for epoxy coatings. *Appl. Clay Sci.* **2021**, *200*, 105890.

(15) Shah, F. U.; Glavatskih, S.; MacFarlane, D. R.; Somers, A.; Forsyth, M.; Antzutkin, O. N. Novel halogen-free chelated orthoborate–phosphonium ionic liquids: synthesis and tribophysical properties. *Phys. Chem. Chem. Phys.* **2011**, *13*, 12865–12873.

(16) Totolin, V.; Minami, I.; Gabler, C.; Dörr, N. Halogen-free borate ionic liquids as novel lubricants for tribological applications. *Tribol. Int.* **2013**, *67*, 191–198.

(17) Zhu, L.; Dong, J.; Ma, Y.; Jia, Y.; Peng, C.; Li, W.; Zhang, M.; Gong, K.; Wang, X. Synthesis and investigation of halogen-free phosphonium-based ionic liquids for lubrication applications. *Tribol. Trans.* **2019**, *62*, 943–954.

(18) Sydow, M.; Owsianiak, M.; Framski, G.; Woźniak-Karczewska, M.; Piotrowska-Cyplik, A.; Ławniczak, Ł.; Szulc, A.; Zgoła-Grześkowiak, A.; Heipieper, H. J.; Chrzanowski, Ł. Biodiversity of soil bacteria exposed to sub-lethal concentrations of phosphonium-based ionic liquids: Effects of toxicity and biodegradation. *Ecotoxicol. Environ. Saf.* **2018**, *147*, 157–164.

(19) Oulego, P.; Blanco, D.; Ramos, D.; Viesca, J.; Díaz, M.; Battez, A. H. Environmental properties of phosphonium, imidazolium and ammonium cation-based ionic liquids as potential lubricant additives. *J. Mol. Liq.* **2018**, *272*, 937–947.

(20) Rohlmann, P.; Munavirov, B.; Furó, I.; Antzutkin, O.; Rutland, M. W.; Glavatskih, S. Non-halogenated ionic liquid dramatically enhances tribological performance of biodegradable oils. *Front. Chem.* **2019**, *7*, 98.

(21) Yu, G.; Yan, S.; Zhou, F.; Liu, X.; Liu, W.; Liang, Y. Synthesis of dicationic symmetrical and asymmetrical ionic liquids and their tribological properties as ultrathin films. *Tribol. Lett.* **2007**, *25*, 197–205.

22

(22) Grace, J.; Vysochanska, S.; Lodge, J.; Iglesias, P. Ionic liquids as additives of coffee bean oil in steel-steel contacts. *Lubricants* **2015**, *3*, 637–649.

(23) Zhou, Y.; Qu, J. Ionic liquids as lubricant additives: a review. *ACS Appl. Mater. Interfaces* **2017**, *9*, 3209–3222.

(24) Reeves, C. J.; Siddaiah, A.; Menezes, P. L. Tribological study of imidazolium and phosphonium ionic liquid-based lubricants as additives in carboxylic acid-based natural oil: advancements in environmentally friendly lubricants. *J. Cleaner Prod.* **2018**, *176*, 241–250.

(25) Yang, J.; Zhou, Z.; Liang, Y.; Tang, J.; Gao, Y.; Niu, J.; Dong, H.; Tang, R.; Tang, G.; Cao, Y. Sustainable Preparation of Microcapsules with Desirable Stability and Bioactivity Using Phosphonium Ionic Liquid as a Functional Additive. *ACS Sustainable Chem. Eng.* **2020**, *8*, 13440–13448.

(26) Reeves, C. J.; Kasar, A. K.; Menezes, P. L. Tribological performance of environmental friendly ionic liquids for high-temperature applications. *J. Cleaner Prod.* **2021**, *279*, 123666.

(27) Tsunashima, K.; Sugiya, M. Physical and electrochemical properties of low-viscosity phosphonium ionic liquids as potential electrolytes. *Electrochem. Commun.* **2007**, *9*, 2353–2358.

(28) Girard, G. M.; Hilder, M.; Zhu, H.; Nucciarone, D.; Whitbread, K.; Zavorine, S.; Moser, M.; Forsyth, M.; Macfarlane, D. R.; Howlett, P. C. Electrochemical and physicochemical properties of small phosphonium cation ionic liquid electrolytes with high lithium salt content. *Phys. Chem. Chem. Phys.* **2015**, *17*, 8706–8713.

(29) Chen, F.; Kerr, R.; Forsyth, M. Cation effect on small phosphonium based ionic liquid electrolytes with high concentrations of lithium salt. *J. Chem. Phys.* **2018**, *148*, 193813.

(30) Meikandan, M.; Ganesh Kumar, P.; Sundarraj, M.; Yogaraj, D. Numerical analysis on heat transfer characteristics of ionic liquids in a tubular heat exchanger. *Int. J. Ambient Energy* **2020**, *41*, 911–917.

(31) Thasneema, K.; Thayyil, M. S.; Rosalin, T.; Elyas, K.; Dipin, T.; Sahu, P. K.; Kumar, N. K.; Saheer, V.; Messali, M.; Hadda, T. B. Thermal and spectroscopic investigations on three phosphonium based ionic liquids for industrial and biological applications. *J. Mol. Liq.* **2020**, *307*, 112960.

(32) Tindale, J. J.; Ragogna, P. J. Highly fluorinated phosphonium ionic liquids: novel media for the generation of superhydrophobic coatings. *Chem. Commun.* **2009**, 1831–1833.

(33) Tindale, J.; Mouland, K.; Ragogna, P. Thiol appended, fluorinated phosphonium ionic liquids as covalent superhydrophobic coatings. *J. Mol. Liq.* **2010**, *152*, 14–18.

(34) Dias, A. M.; Marceneiro, S.; Braga, M. E.; Coelho, J. F.; Ferreira, A. G.; Simões, P. N.; Veiga, H. I.; Tomé, L. C.; Marrucho, I. M.; Esperança, J. M., et al. Phosphonium-based ionic liquids as modifiers for biomedical grade poly (vinyl chloride). *Acta Biomater.* **2012**, *8*, 1366–1379.

(35) Nguyen, T. K. L.; Livi, S.; Pruvost, S.; Soares, B. G.; Duchet-Rumeau, J. Ionic liquids as reactive additives for the preparation and modification of epoxy networks. *J. Polym. Sci., Part A: Polym. Chem.* **2014**, *52*, 3463–3471.

(36) Yousfi, M.; Livi, S.; Duchet-Rumeau, J. Ionic liquids: A new way for the compatibilization of thermoplastic blends. *Chem. Eng. J.* **2014**, *255*, 513–524.

(37) Lins, L. C.; Livi, S.; Duchet-Rumeau, J.; Gérard, J.-F. Phosphonium ionic liquids as new compatibilizing agents of biopolymer blends composed of poly (butylene-adipate-co-terephtalate)/poly (lactic acid)(PBAT/PLA). *RSC advances* **2015**, *5*, 59082–59092.

(38) Soares, B. G.; Silva, A. A.; Pereira, J.; Livi, S. Preparation of epoxy/Jeffamine networks modified with phosphonium based ionic liquids. *Macromol. Mater. Eng.* **2015**, *300*, 312–319.

(39) Westerholt, A.; Weschta, M.; Bosmann, A.; Tremmel, S.; Korth, Y.; Wolf, M.; Schlucker, E.; Wehrum, N.; Lennert, A.; Uerdingen, M., et al. Halide-free synthesis and tribological performance of oil-miscible ammonium and phosphonium-based ionic liquids. *ACS Sustainable Chem. Eng.* **2015**, *3*, 797–808.

(40) Blanco, D.; Bartolome, M.; Ramajo, B.; Viesca, J.; Gonzalez, R.; Hernandez Battez, A. Wetting properties of seven phosphonium cation-based ionic liquids. *Ind. Eng. Chem. Res.* **2016**, *55*, 9594–9602.

(41) Batchelor, T.; Cunder, J.; Fadeev, A. Y. Wetting study of imidazolium ionic liquids. *J. Colloid Interface Sci.* **2009**, *330*, 415–420.

(42) Pameijer, C. H.; Glantz, P.-O.; von Fraunhofer, A. Clinical and Technical Considerations of Luting Agents for Fixed Prosthodontics. *Int. J. Dent.* **2012**,

(43) Kalin, M.; Polajnar, M. The effect of wetting and surface energy on the friction and slip in oil-lubricated contacts. *Tribol. Lett.* **2013**, *52*, 185–194.

(44) Liu, T.; Wang, K.; Chen, Y.; Zhao, S.; Han, Y. Dominant role of wettability in improving the specific capacitance. *Green Energy Environ.* **2019**, *4*, 171–179.

(45) Grundke, K.; Bogumil, T.; Werner, C.; Janke, A.; Pöschel, K.; Jacobasch, H.-J. Liquid-fluid contact angle measurements on hydrophilic cellulosic materials. *Colloids Surf., A* **1996**, *116*, 79–91.

(46) Uelzen, T.; Müller, J. Wettability enhancement by rough surfaces generated by thin film technology. *Thin Solid Films* **2003**, *434*, 311–315.

(47) Matczak, L.; Johanning, C.; Gil, E.; Guo, H.; Smith, T. W.; Schertzer, M.; Iglesias, P. Effect of cation nature on the lubricating and physicochemical properties of three ionic liquids. *Tribol. Int.* **2018**, *124*, 23–33.

(48) Zhang, W.; Jiang, S.; Sun, J.; Wu, Z.; Qin, T.; Xi, X. Wettability of coal by room temperature ionic liquids. *Int. J. Coal Prep. Util.* **2021**, *41*, 418–427.

(49) Tiago, G.; Restolho, J.; Forte, A.; Colaço, R.; Branco, L.; Saramago, B. Novel ionic liquids for interfacial and tribological applications. *Colloids Surf., A* **2015**, *472*, 1–8.

(50) Carrera, G. V.; Afonso, C. A.; Branco, L. C. Interfacial properties, densities, and contact angles of task specific ionic liquids. *J. Chem. Eng. Data* **2010**, *55*, 609–615.

(51) Cigno, E.; Magagnoli, C.; Pierce, M. S.; Iglesias, P. Lubricating ability of two phosphonium-based ionic liquids as additives of a bio-oil for use in wind turbines gearboxes. *Wear* **2017**, *376*, 756–765.

(52) Zhao, X.; Zhu, Y.; Zhang, C.; Lei, J.; Ma, Y.; Du, F. Positive charge pesticide nanoemulsions prepared by the phase inversion composition method with ionic liquids. *RSC advances* **2017**, *7*, 48586–48596.

(53) Malali, S.; Foroutan, M. Study of wetting behavior of BMIM+/PF6–ionic liquid on TiO2 (110) surface by molecular dynamics simulation. *J. Phys. Chem. C* **2017**, *121*, 11226–11233.

(54) Bordes, E.; Douce, L.; Quitevis, E. L.; Pádua, A. A.; Costa Gomes, M. Ionic liquids at the surface of graphite: Wettability and structure. *J. Chem. Phys.* **2018**, *148*, 193840.

(55) Bhattacharjee, S.; Khan, S. Effect of alkyl chain length on the wetting behavior of imidazolium based ionic liquids: A molecular dynamics study. *Fluid Phase Equilib.* **2019**, *501*, 112253.

(56) Bhattacharjee, S.; Khan, S. The wetting behavior of aqueous imidazolium based ionic liquids: a molecular dynamics study. *Phys. Chem. Chem. Phys.* **2020**, *22*, 8595–8605.

(57) Atkinson, H.; Bara, J. E.; Turner, C. H. Molecular-level analysis of the wetting behavior of imidazolium-based ionic liquids on bismuth telluride surfaces. *Chem. Eng. Sci.* **2020**, *211*, 115270.

(58) Bahrami, M.; Ghatee, M. H.; Ayatollahi, S. F. Simulation of Wetting and Interfacial Behavior of Quaternary Ammonium and Phosphonium Ionic Liquid Nanodroplets Over Face-Centered Cubic Metal Surfaces. *J. Phys. Chem. B* **2020**, *124*, 2835–2847.

(59) Castejon, H. J.; Wynn, T. J.; Marcin, Z. M. Wetting and tribological properties of ionic liquids. *J. Phys. Chem. B* **2014**, *118*, 3661–3668.

(60) Liu, H.; Jiang, L. Wettability by ionic liquids. *Small* **2016**, *12*, 9–15.

(61) Manoj, A.; Kasar, A. K.; Menezes, P. L. Tribocorrosion of porous titanium used in biomedical applications. *J. Bio- Tribo-Corros.* **2019**, *5*, 1–16.

(62) Egorov, V. M.; Djigailo, D. I.; Momotenko, D. S.; Chernyshov, D. V.; Toroches-nikova, I. I.; Smirnova, S. V.; Pletnev, I. V. Task-specific ionic liquid trioctylmethylammonium salicylate as extraction solvent for transition metal ions. *Talanta* **2010**, *80*, 1177–1182.

(63) Kasar, A. K.; Reeves, C. J.; Menezes, P. L. The effect of particulate additive mixtures on the tribological performance of phosphonium-based ionic liquid lubricants. *Tribol. Int.* **2022**, *165*, 107300.

(64) Jorgensen, W. L.; Maxwell, D. S.; Tirado-Rives, J. Development and testing of the OPLS all-atom force field on conformational energetics and properties of organic liquids. *J. Am. Chem. Soc.* **1996**, *118*, 11225–11236.

(65) Dodda, L. S.; Cabeza de Vaca, I.; Tirado-Rives, J.; Jorgensen, W. L. LigParGen web server: an automatic OPLS-AA parameter generator for organic ligands. *Nucleic Acids Res.* **2017**, *45*, W331–W336.

(66) Maghfiroh, C.; Arkundato, A.; Maulina, W., et al. Parameters (σ, ε) of Lennard-Jones for Fe, Ni, Pb for Potential and Cr based on Melting Point Values Using the Molecular Dynamics Method of the Lammps Program. J. Phys.: Conf. Ser. 2020; p 012022.

(67) Delhommelle, J.; Millié, P. Inadequacy of the Lorentz-Berthelot combining rules for accurate predictions of equilibrium properties by molecular simulation. *Molecular Physics* **2001**, *99*, 619–625.

(68) Herrera, C.; Garcia, G.; Atilhan, M.; Aparicio, S. Nanowetting of graphene by ionic liquid droplets. *J. Phys. Chem. C* **2015**, *119*, 24529–24537.

(69) Burt, R.; Birkett, G.; Salanne, M.; Zhao, X. Molecular dynamics simulations of the influence of drop size and surface potential on the contact angle of ionic-liquid droplets. *J. Phys. Chem. C* **2016**, *120*, 15244–15250.

(70) Guan, Y.; Shao, Q.; Chen, W.; Liu, S.; Zhang, X.; Deng, Y. Dynamic three-dimensional nanowetting behavior of imidazolium-based ionic liquids probed by molecular dynamics simulation. *J. Phys. Chem. C* **2017**, *121*, 23716–23726.

(71) Martínez, L.; Andrade, R.; Birgin, E. G.; Martínez, J. M. PACKMOL: a package for building initial configurations for molecular dynamics simulations. *J. Comput. Chem.* **2009**, *30*, 2157–2164.

(72) Plimpton, S. Fast parallel algorithms for short-range molecular dynamics. *J. Comput. Phys.* **1995**, *117*, 1–19.

(73) Evans, D. J.; Holian, B. L. The nose–hoover thermostat. *J. Comput. Phys.* **1985**, *83*, 4069–4074.

(74) Spreiter, Q.; Walter, M. Classical molecular dynamics simulation with the Velocity Verlet algorithm at strong external magnetic fields. *J. Comput. Phys.* **1999**, *152*, 102–119.

(75) Santiso, E. E.; Herdes, C.; Müller, E. A. On the calculation of solid-fluid contact angles from molecular dynamics. *Entropy* **2013**, *15*, 3734–3745.

(76) Khalkhali, M.; Kazemi, N.; Zhang, H.; Liu, Q. Wetting at the nanoscale: A molecular dynamics study. *J. Chem. Phys.* **2017**, *146*, 114704.

(77) Yuan, Y.; Lee, T. R. In *Surf. Sci. techniques*; Bracco, G., Holst, B., Eds.; Springer Berlin Heidelberg: Berlin, Heidelberg, 2013; pp 3–34.

(78) Liu, F.; Shen, W. Forced wetting and dewetting of liquids on solid surfaces and their roles in offset printing. *Colloids Surf., A* **2008**, *316*, 62–69.

(79) Aliaga, C.; Baldelli, S. A sum frequency generation study of the room-temperature ionic liquid- titanium dioxide interface. *J. Phys. Chem. C* **2008**, *112*, 3064–3072.

(80) Xu, S.; Xing, S.; Pei, S.-S.; Baldelli, S. Sum frequency generation spectroscopy study of an ionic liquid at a graphene-BaF2 (111) interface. *J. Phys. Chem. B* **2014**, *118*, 5203–5210.

(81) Guo, Q.; Cocks, I.; Williams, E. The adsorption of benzoic acid on a TiO2 (110) surface studied using STM, ESDIAD and LEED. *Surf. Sci.* **1997**, *393*, 1–11.

(82) Perry, C.; Haq, S.; Frederick, B.; Richardson, N. Face specificity and the role of metal adatoms in molecular reorientation at surfaces. *Surf. Sci.* **1998**, *409*, 512–520.

(83) Frederick, B.; Leibsle, F.; Haq, S.; Richardson, N. Evolution of lateral order and molecular reorientation in the benzoate/Cu (110) system. *Surf. Rev. Lett.* **1996**, *3*, 1523–1546.

(84) Morosanova, M. A.; Morosanova, E. I. Silica-titania xerogel for solid phase spectropho-
tometric determination of salicylate and its derivatives in biological liquids and phar-
maceuticals. *Chem. Cent. J.* **2015**, *9*, 1–8.

(85) Imai, Y.; Kamada, J.-i. Vibrational spectra of saccharin nitranion and its orientation
on the surface of silver metal particles. *Spectrochim. Acta, Part A* **2005**, *61*, 711–715.

TOC Graphic